Target Separation from Sabot with Permanent Magnetic Array and Beam Steering Method with Four-Wave Mixing*)

Nobukazu KAMEYAMA and Hiroki YOSHIDA
Gifu University, 1-1 Yanagido, Gifu, Gifu 501-1193, Japan

(Received 31 May 2012 / Accepted 27 September 2012)

We developed the permanent magnet array to separate a target from a sabot and analyzed the deceleration of the sabot velocity per unit length. The injection accuracy is about ± 12 mm at one meter from the injector muzzle when the sabot velocity is around 30 m/s. The method of compensation of a phase conjugate beam with four-wave mixing is shown. As one pump beam for four-wave mixing has a bit of longitudinal angle from the plane that another pump beam and a seed beam propagate, the phase conjugate beam tilts at the same angle from the plane. The displacement angle of the phase conjugate beam is compensated by adequately adjusting the angle between two pump beams.

Keywords: injector, target separation, beam steering, four-wave mixing

DOI: 10.1585/pfr.8.3404045

1. Introduction

Fusion targets are provided to one modular chamber at 300 m/s and 4 Hz [1]. The target is protected with a sabot during the acceleration and the sabot must be separated before the target enters the chamber. The methods to use deceleration coils or sabots that have a separation feature [2] are researched as the methods of the sabot separation. In these methods, it is necessary to control the deceleration timing. In this paper, we show the method of decelerating a sabot to separate a target with a permanent magnet array (PMA) as the way to utilize fixed magnetic field where any control is not necessary.

A fusion reaction occurs by irradiating high-energy laser beams to a target at the point on which all laser beams are focused. Since an injected target has a displacement from the focal point, many methods to irradiate the target with laser beams have been proposed. One of the candidates is the control of the trajectory of a target [3, 4]. Another is to steer laser beams. In the case of the beam steering, there are mainly two methods. One is to use active mirrors [5] and another to use phase conjugate (PC) mirrors [6]. In the former method, it is necessary to measure the target velocity and the direction and to predict the arriving position in the chamber. The active mirrors are adjusted with the prediction results. The disadvantages of this method are the complexities (1) of the equipment for the measurement and the prediction and (2) of the control of mirrors over 100 kg at high repetition. In the latter method, some probe laser beams whose total energies are low enough not to damage a target are irradiated first. The scattered beam by the target enters into a PC mirror.

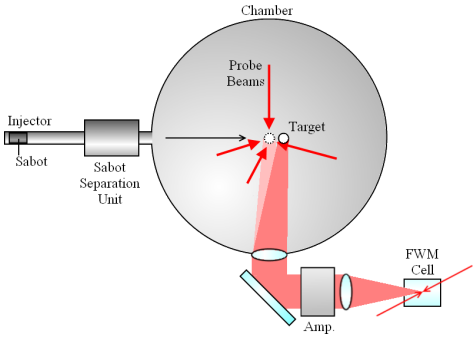

Fig. 1 Schematic view of IFE with beam steering compensation by FWM.

The reflected beam is called a PC beam and has the conjugate phase of an incident beam into a PC mirror. The PC beam originated from the beam scattered by the target retraces the same path of the scattered one and goes back to the same point at which the probe beams are scattered by the target. Therefore the precise measurement and the prediction of the target position are unnecessary in this way. One just controls the timing of irradiation of the target with probe beams. The target has moved several hundred micrometers when the PC beam comes back because the target is shot at 300 m/s and the length of the laser chain is about one hundred meters. The PC beam has to be compensated to irradiate the target accurately. We show the method of adjusting the PC beam with four-wave mixing (FWM) in principle. Figure 1 shows a schematic diagram of target injection system with four-wave mixing that is used instead of the PC mirror. The compensation of the PC beam is confirmed experimentally.

author's e-mail: q3814101@edu.gifu-u.ac.jp

*) This article is based on the presentation at the Conference on Inertial Fusion Energy '12.

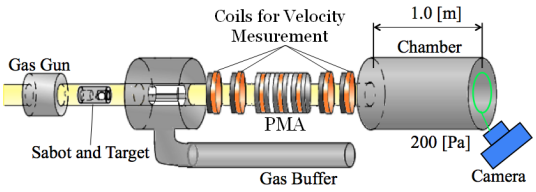

Fig. 2 Experimental equipment of the injection system.

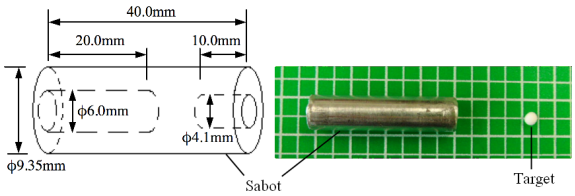

Fig. 3 The structure of the sabot and the target.

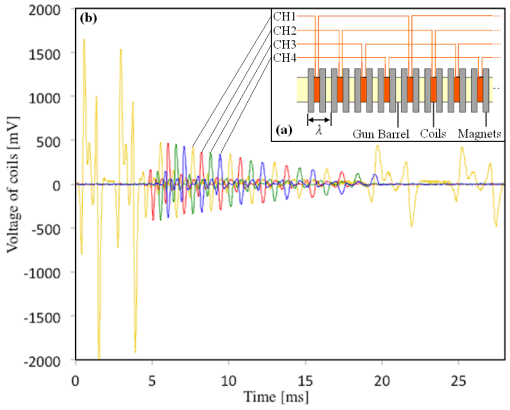

Fig. 4 (a) The arrangement of the PMA; (b) the voltage waveform obtained by the coils.

2. Injection

2.1 Experimental equipment

The experimental equipment of the injection system is shown in Fig. 2. It is constructed with a gas gun whose inner diameter (ID) is 9.4 mm, a gas buffer, a PMA and a chamber whose length is one meter. Figure 3 shows the structure of the sabot (duralumin; 5.07-gram; electric resistivity, 6.0×10^{-5} Ωm) and the target (foam polystyrene; 0.8 mg; diameter, 4 mm). Before and behind the PMA, there are two pairs of a coil and a magnet to measure the sabot velocity before and after deceleration, respectively. One can obtain the sabot velocities by traveling time of it passing through the pairs of them. The sabot with the target is shot by the gas gun, passing through the PMA, being decelerated by it. Part (a) in Fig. 4 shows the arrangement of the PMA. It is constructed with 40 permanent magnets (neodymium magnet; 316 mT on its surface; thickness, 5 mm) whose north and south poles are arranged alternately at five mm intervals. The 20 coils to measure the sabot velocity are wound on the gun barrel between the magnets. Part (b) shows the voltage waveform obtained when the sabot passed through the PMA. One can calculate the sabot velocity in the PMA with the traveling time between two peeks of the waveform and the one cycle of the magnets λ. The pressure in the chamber is 200 Pa. The injection accuracy is measured at the point one meter from the gun muzzle with a high-speed camera (Canon EX-F1).

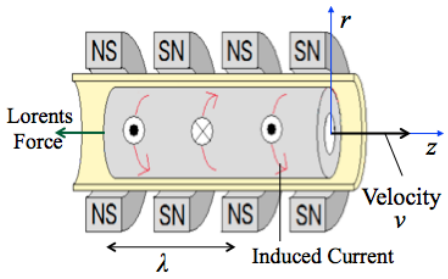

Fig. 5 Analytical model of sabot deceleration with PMA.

2.2 Theory of deceleration with PMA

Figure 5 shows an analytical model of sabot deceleration with a PMA. When a sabot is passing through it, an induced current is generated. In the opposite direction of the sabot, a Lorentz force arises from the induced current and the magnetic field and decelerates it.

When the magnetic flux density $\boldsymbol{B}$ can be written as

$$\boldsymbol{B} = B_r \boldsymbol{e}_r + B_z \boldsymbol{e}_z = B_0(r) \sin \frac{2\pi z}{\lambda} \boldsymbol{e}_r + B_z(r, z) \boldsymbol{e}_z, \quad (1)$$

where B_r and B_z are, respectively, the r- and z-components of $\boldsymbol{B}$, and $B_0(r)$ and λ are, respectively, the amplitude and wavelength of the sinusoidal variation of B_r in z-direction, the force acting on a sabot in z-direction F_z can be written in a cylindrical coordinate (r, θ, z) as follows.

$$\begin{aligned}
F &= \frac{\boldsymbol{F} \cdot \boldsymbol{v}_s}{v_s} = \iiint_{\text{Sabot}} \frac{\boldsymbol{f} \cdot \boldsymbol{v}_s}{v_s} \mathrm{d}r(r\mathrm{d}\theta)\mathrm{d}z \\
&= \iiint_{\text{Sabot}} \frac{(\boldsymbol{i}_s \times \boldsymbol{B}) \cdot \boldsymbol{v}_s}{v_s} \mathrm{d}r(r\mathrm{d}\theta)\mathrm{d}z \\
&= \iiint_{\text{Sabot}} \frac{[(\boldsymbol{v}_s \times \boldsymbol{B}) \times \boldsymbol{B}] \cdot \boldsymbol{v}_s}{\rho v_s} \mathrm{d}r(r\mathrm{d}\theta)\mathrm{d}z \\
&= \iiint_{\text{Sabot}} \frac{|\boldsymbol{v}_s \times \boldsymbol{B}|^2}{\rho v_s} \mathrm{d}r(r\mathrm{d}\theta)\mathrm{d}z \\
&= \iiint_{\text{Sabot}} \frac{-v_s^2 B_r^2}{\rho v_s} \mathrm{d}r(r\mathrm{d}\theta)\mathrm{d}z \\
&= -\frac{v_s}{\rho} \iiint_{\text{Sabot}} B_r^2 \mathrm{d}r(r\mathrm{d}\theta)\mathrm{d}z \\
&= -\frac{v_s}{\rho} \int_0^{2\pi} \mathrm{d}\theta \int_0^{n\lambda} \sin^2\left(\frac{2\pi z}{\lambda}\right)\mathrm{d}z \int_{r_{si}}^{r_{so}} r B_0^2(r)\mathrm{d}r \\
&= \frac{-\pi n \lambda v_s}{\rho} \int_{r_{si}}^{r_{so}} r B_0^2(r)\mathrm{d}r, \qquad (2)
\end{aligned}$$

where $\boldsymbol{F}$ is the force acting on the sabot, $\boldsymbol{v}_s = v_s \boldsymbol{e}_z$ is the flight velocity of the sabot, $\boldsymbol{f}$ is the force acting on a unit

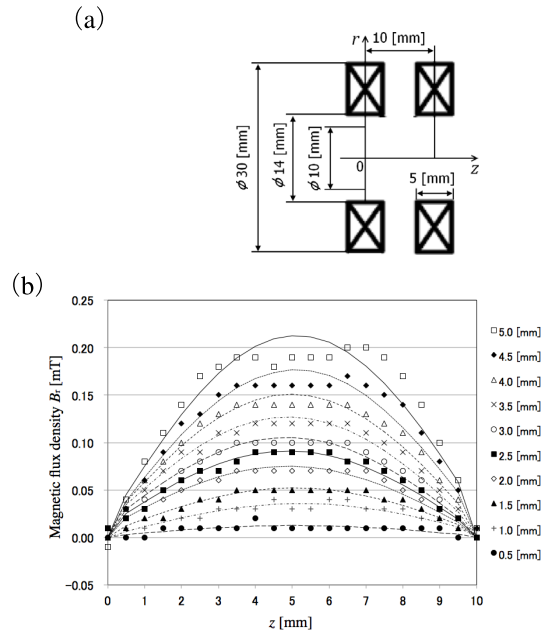

Fig. 6 Measurement of magnetic flux density. (a) Measured space of magnetic flux density. (b) Measured and approximated magnetic flux density in the PMA.

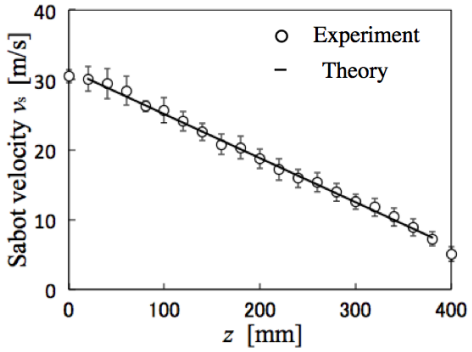

Fig. 7 Experimental results of sabot deceleration with the theoretical line.

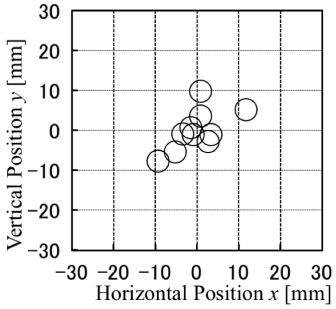

Fig. 8 Injection accuracy of the targets separated from the sabot.

volume of the sabot, $\boldsymbol{i}_s$ is the density of the induced current in the sabot, and ρ is electrical resistivity of the sabot. From $\mathrm{d}z/\mathrm{d}t = v_s$,

$$\frac{\mathrm{d}v_\mathrm{s}}{\mathrm{d}z} = \frac{1}{\mathrm{d}z/\mathrm{d}t}\frac{\mathrm{d}v_s}{\mathrm{d}t} = \frac{F}{mv_\mathrm{s}} = \frac{-\pi n\lambda}{m\rho}\int_{r_\mathrm{si}}^{r_\mathrm{so}} rB_0^2(r)\mathrm{d}r. \quad (3)$$

The sabot is decelerated linearly with respect to the sabot direction so that the right side (3) is constant.

The magnetic flux in the magnets as shown in part (a) of Fig. 6 is measured at intervals of 0.5 mm in both r- and z-axial direction. Part (b) shows the measured and the approximated magnetic flux density in the PMA. The markers show the measured magnetic flux density. The lines show the magnetic flux density approximated by sine waves. The deceleration per unit length calculated from (3) and the approximated values is 63.1 (m/s)/m.

2.3 Experimental results

Figure 7 shows the theoretical and experimental results of the sabot deceleration. The straight line shows the theoretical results, and open circles the experimental ones. The sabot is decelerated linearly and the deceleration per unit length is 63.6 (m/s)/m. This result coincides with the theoretical one with 0.8% accuracy.

Figure 8 shows the injection accuracy of the injection system. The injection accuracy is about ±12 mm at the sabot velocity 30 m/s before deceleration.

3. Beam steering

3.1 Way of the compensation of a PC beam angle with FWM

FWM is one of the nonlinear optical effects that generate a PC beam like Stimulated Brillouin Scattering (SBS) [7]. Figure 9 shows the vector diagram of four beams of FWM. The PC beam is generated in the opposite direction of the seed beam by irradiating a seed beam to a FWM cell where two pump beams are counter-propagating as shown in the left of Fig. 9 (a). In the case that one pump beam tilts longitudinally at a small angle $\mathrm{d}\theta$ from the plane in which another pump beam and the seed beam lie, the PC beam has the same angle from the plane as indicated in the right of Fig. 9 (b).

Figure 10 shows a schematic diagram of compensation of a PC beam angle with FWM. There are two lenses whose focal length are f_0 and f_1 between a target and a FWM cell. d shows the distance between the target and the focal lengths of L_0 and L that of two lenses. The scattered beam by the target passes through two lenses, being focused into the cell. The PC beam is generated and propagates in the opposite direction tilting at the angle $\mathrm{d}\theta$ from the seed beam and comes back to the point at the distance δ from the position at which probe beams are scattered. The displacement of a PC beam at L_1 is written as $f_1\ \mathrm{d}\theta$, provided that the PC beam is generated at the focal point of lens L_1. The δ is given by

$$\delta = \frac{d}{f_0} f_1 \cdot \mathrm{d}\theta.$$

This δ is independent of light path L.

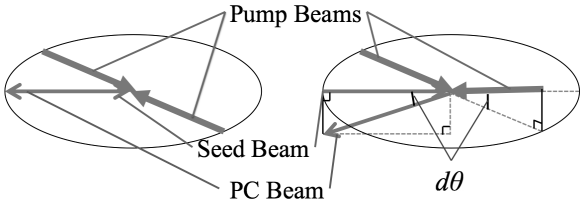

(a) counter-propagating (b) non-counter propagating

Fig. 9 Vector diagram of FWM.

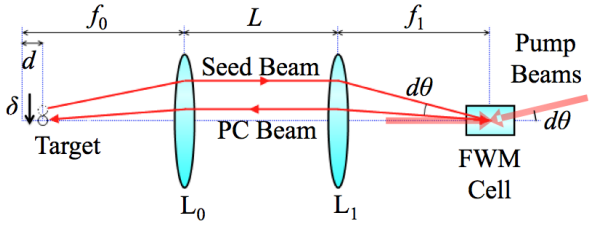

Fig. 10 Schematic view of compensation of a PC beam angle with FWM in two lenses system.

3.2 Experiment to confirm the compensation of a PC beam angle

Figure 11 shows the experimental equipment to confirm the compensation of a PC beam angle. Nd: YAG laser (wavelength is 1064 nm, pulse width 5~7 ns) is used as the source of pump beams and a seed beam. The first pump beam passes through the wedged-beam splitter WBS1 and is focused by the lens L2 whose focal length is 600 mm into the FWM cell that contains Nitrobenzene used as the material of FWM. The second pump beam is obtained by retro-reflecting it with the mirror M. The reflected beam by WBS1 passes through the pinhole PH1 whose diameter is one millimeter; WBS2 and PH2, being focused by L1 whose focal length is 200 mm into the cell as a seed beam. The PC beam is generated in the opposite direction of the seed beam, reflected by WBS2 and monitored with the camera (ELECOM UCAM-DLK130T). With M to obtain the second pump beam, the second pump beam is adjusted at a small angle in the direction perpendicular to the plane in which the first beam and the seed beam lie.

3.3 Results of the compensation of a PC beam angle with FWM

Figures 12 (a) and (b) show the results that dθ is set at 2.5 mrad and 0.0 mrad respectively. In the arrangement, the compensation of the PC beam is given by multiplying the focal length of L1 by dθ. Since the displacement and the focal length are 0.46 mm and 200 mm respectively, the compensated angle of the PC beam is 2.3 mrad. This value is in good agreement with that of the results. As a result, setting the angle between two pump beams compensates the moving distance of a target.

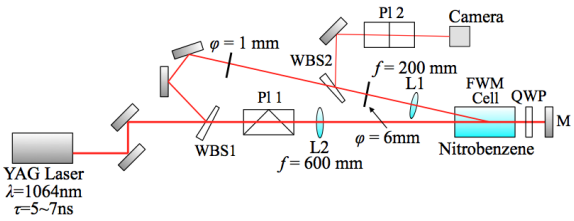

Fig. 11 Experimental equipment to confirm the compensation of a PC beam angle: WBS, wedged beam splitter; Pl, Polarizer; L, lens; PH, pinhole; QWP, quarter wave plate; M, mirror.

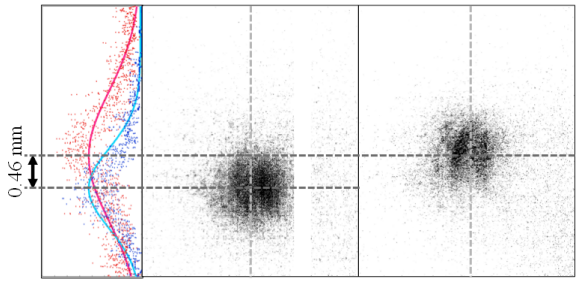

(a) dθ = 2.5 mrad (b) dθ = 0.0 mrad

Fig. 12 Compensation results of the PC beam angle.

4. Conclusion

We showed the separation of the target from the sabot with the PMA. The deceleration of the sabot velocity agrees with the theoretical value. The target can be separated from the sabot with the PMA by adequately designing the length even where the velocity is 300 m/s.

The angle between the PC beam and the seed beam correspond to that of the two pump beams. It is confirmed that setting the angle between two pump beams compensates the displacement of the target. The compensation of the PC beam is dependent on the angle between two pump beams, focal lengths of lenses and the distance of the target to the focal length of final optics but not light path.

[1] Committee of design of IFE reactor, *Conceptional design of power generating plant with fast ignition* (Institute of laser engineering, Osaka university, IFE forum, 2006).
[2] D.T. Goddin *et al.*, Fusion Eng. Des. **60**, 27 (2002).
[3] T. Kassai and R. Tsuji, J. Phys.: Conf. Ser. **112**, 032047 (2008).
[4] R. Petzoldt *et al.*, Fusion Sci. Technol. **52**, 459 (2007).
[5] L. Carlson *et al.*, Fusion Sci. Technol. **56**, 409 (2009).
[6] M. Kalal *et al.*, J. Fusion Energy **29**, 527 (2010).
[7] A. Yariv and P. Yeh, *Photonics: optical electronics in modern communication 6th ed.* (Oxford University Press, New York, 2007) p. 387.